Editors' Suggestion

Predicted Pressure-Induced Superconducting Transition in Electride Li_6P

Ziyuan Zhao,[1,*] Shoutao Zhang,[1,*] Tong Yu,[1] Haiyang Xu,[1] Aitor Bergara,[2,3,4,†] and Guochun Yang[1,‡]
[1]*Centre for Advanced Optoelectronic Functional Materials Research and Laboratory for UV Light-Emitting Materials and Technology of Ministry of Education, Northeast Normal University, Changchun 130024, China*
[2]*Departamento de Física de la Materia Condensada, Universidad del País Vasco-Euskal Herriko Unibertsitatea, UPV/EHU, 48080 Bilbao, Spain*
[3]*Donostia International Physics Center (DIPC), 20018 Donostia, Spain*
[4]*Centro de Física de Materiales CFM, Centro Mixto CSIC-UPV/EHU, 20018 Donostia, Spain*

(Received 7 November 2018; published 7 March 2019)

Electrides are unique compounds where most of the electrons reside at interstitial regions of the crystal behaving as anions, which strongly determines its physical properties. Interestingly, the magnitude and distribution of interstitial electrons can be effectively modified either by modulating its chemical composition or external conditions (e.g., pressure). Most of the electrides under high pressure are nonmetallic, and superconducting electrides are very rare. Here we report that a pressure-induced stable Li_6P electride, identified by first-principles swarm structure calculations, becomes a superconductor with a predicted superconducting transition temperature T_c of 39.3 K, which is the highest among the already known electrides. The interstitial electrons in Li_6P, with dumbbell-like connected electride states, play a dominant role in the superconducting transition. Other Li-rich phosphides, Li_5P, $Li_{11}P_2$, $Li_{15}P_2$, and Li_8P, are also predicted to be superconducting electrides, but with a lower T_c. Superconductivity in all these compounds can be attributed to a combination of a weak electronegativity of phosphorus (P) with a strong electropositivity of lithium (Li), and opens up the interest to explore high-temperature superconductivity in similar binary compounds.

DOI: 10.1103/PhysRevLett.122.097002

Electrides represent a class of extraordinary compounds where some electrons in the solid are localized at interstitial regions, rather than being attached to atoms, and behave as anions [1,2]. The existence of quantized orbitals at the interstitials allows the transfer of electrons there [3]. Although the energies of both interstitial and atomic orbitals increase with pressure, the change of the interstitial orbital energy is usually smaller than that of the atomic orbital [4,5]. Thus, formation of electrides can become energetically favorable under high pressure, and various electrides have been already induced by pressure both in elements [6–9] and compounds [10–12]. These interstitial electrons largely determine the physical properties of the electrides [13–15].

Searching for high-temperature superconductivity remains one of the most important topics in condensed matter physics. Even though cuprates [16,17] and iron pnictides [18,19], among others, took a leading role on this pursuit, it is well known that pressure enhances the superconducting properties [20,21], and hydrogen sulfides [22–24], phosphorus hydrides [25–29], and lanthanum hydrides [30–32] have been recently observed to be high-temperature superconductors.

On the other hand, even though electrides are usually insulators, recent experiments showed that a canonical electride $[Ca_{24}Al_{28}O_{64}]^{4+}(e^-)_4$ becomes a superconductor ($T_c \sim 0.4$ K) [33–36]. The interstitial electrons in $Ca_{24}Al_{28}O_{64}$ accommodate loosely in the cages of unit structures, rising up an uncommon conductivity [35]. Additionally, Mn_5Si_3-type Nb_5Ir_3 [15] and two-dimensional Y_2C [37] have been also found to hold both electride states and superconductivity. Additionally, as stated above, it is well known that pressure induces the formation of electrides. For example, both alkaline and alkaline-earth metals form electrides under pressure, as s orbital electrons can easily go to interstitial sites [4]. The strong localization of both interstitial and orbital electrons, caused by orbital coupling, makes them insulating [8,38–41]. However, under higher pressure Li shows a phase transition to a metallic phase while keeping the electride state (*Cmca*-24 Li at 90 GPa) [42]. Although this is a poor metal, the inclusion of extra elements might adjust interstitial electrons and help to improve its metallic character. For instance, as it was observed in suboxide Li_6O [43] and Ca_2N-type Li_4N [13] electrides, filling free spaces of Li with guest p-block elements modifies the electronic band topology and even increases its superconducting T_c.

Having this in mind, and considering that phosphorus (P) has a moderate electronegativity and it is a remarkable superconductor [44,45], Li phosphides have reasonable

expectances to become superconducting electrides. At ambient conditions the stable Li-P binary compounds (i.e., LiP_7, LiP_5, Li_3P_7, LiP, and Li_3P) are nonmetal, and show great potential applications in lithium ion batteries [46,47]. Theoretical calculations have provided a deep insight on the structural and electronic evolution of P anodes during the lithiation [48]. Moreover, Li–P-doped phases with aluminum become metallic, which is important to optimize the electrochemical performance of P anodes [48]. Interestingly, in a recent work a Li_5P metallic electride has been found to be stable under pressure [49]. Li atoms in Li_5P donate the excess electrons into the lattice spaces, forming an unusual 2D electride, with convenient conducting electronic channels.

These distinguishing electronic properties have attracted our attention of Li-P compounds. Herein, compounds with Li_xP_y stoichiometry have been searched from 50 to 300 GPa, and several superconducting electrides (i.e., $C2/c$ Li_5P, $Cmcm$ Li_5P, P-1 $Li_{11}P_2$, P-1 Li_6P, $C2/c$ Li_6P, $C2/m$ $Li_{15}P_2$, and $C2/c$ Li_8P) have been found under pressure. In these electrides, electrons gather not only at interstitial sites but also around P atoms. Notably, the superconducting properties of the electrides are determined by their structural configurations (Li_5P, $Li_{11}P_2$, Li_6P, $Li_{15}P_2$, and Li_8P). $C2/c$ Li_6P, with more connected interstitial electrons, shows the highest T_c value of 39.3 K, which becomes the highest predicted T_c between already reported electrides.

To search the thermodynamically stable candidates of Li-P alloys under pressure, we have employed the swarm-intelligence based CALYPSO structure prediction method, which can efficiently find the stable structures just depending on the given chemical compositions [50,51]. Structural optimization and electronic property calculations were performed in the framework of density functional theory (DFT) [52,53] within the Perdew-Burke-Ernzerhof of the generalized gradient approximation (GGA) [54] as implemented in the VASP5.3 code [55]. The electron-ion interaction is described by pseudopotentials built within the scalar relativistic projector augmented wave (PAW) [56] method with $3s^23p^3$ valence electrons for P, and $1s^22s^12p^0$ valence electrons for Li. A cutoff energy of 500 eV and Monkhorst-Pack k meshes [57] with a grid spacing of $2\pi \times 0.025$ Å^{-1} were used to yield a good convergence for the enthalpy. Dynamic stability and superconducting properties were calculated based on density functional perturbation theory and the plane-wave pseudopotential method with Vanderbilt-type ultrasoft pseudopotentials, as implemented in the QUANTUM ESPRESSO code [58]. Detailed descriptions of structural predictions and computational details can be found in the Supplemental Material [59].

Various Li-rich phosphides (Li_xP_y, $x = 1-8$, and $y = 1$; $x = 3$, 5, 7, 9, 11, 13, 15, and $y = 2$; $x = 4$, 5, 7, and $y = 3$) have been searched extensively. Herein, structure prediction calculations were performed at 0 K and selected pressures of 50, 100, 200, and 300 GPa. The relative thermodynamic stability of Li_xP_y stoichiometries at 100, 200, and 300 GPa is shown in Fig. 1(a), and that at 50 GPa is in Fig. S1 of the Supplemental Material [59]. Stable phases lie on the global stability line of the convex hull, whereas compounds lying on the dotted lines are metastable with respect to decomposition into other Li_xP_y compounds or elemental Li and P solids. In addition to the stable LiP (from 63 up to 300 GPa), other Li-rich stoichiometries (Li_3P, Li_7P_2, Li_5P, $Li_{11}P_2$, Li_6P, $Li_{15}P_2$, and Li_8P) are predicted to be stable under increased pressure. The most stable Fm-3m Li_3P lies on the convex hulls at the whole pressure range. P-3m1 Li_7P_2 is stable between 154–300 GPa. Additionally, $P6/mmm$ Li_5P starts to be stable at 10.3 GPa [49], and remains stable until 163 GPa. There are two other Li_5P stable phases with increasing pressure: $C2/c$ Li_5P is stable between 163 and 249 GPa, while $Cmcm$ Li_5P stabilizes above 249 GPa. P-1 $Li_{11}P_2$ is stable above 195 GPa. For the stoichiometries with a higher Li content, Li_6P, $Li_{15}P_2$, and Li_8P become stable over 178, 266, and 150 GPa, respectively. P-1 Li_6P transfers to $C2/c$ Li_6P above 271 GPa. The pressure-composition phase diagram is shown in Fig. 1(b). All the

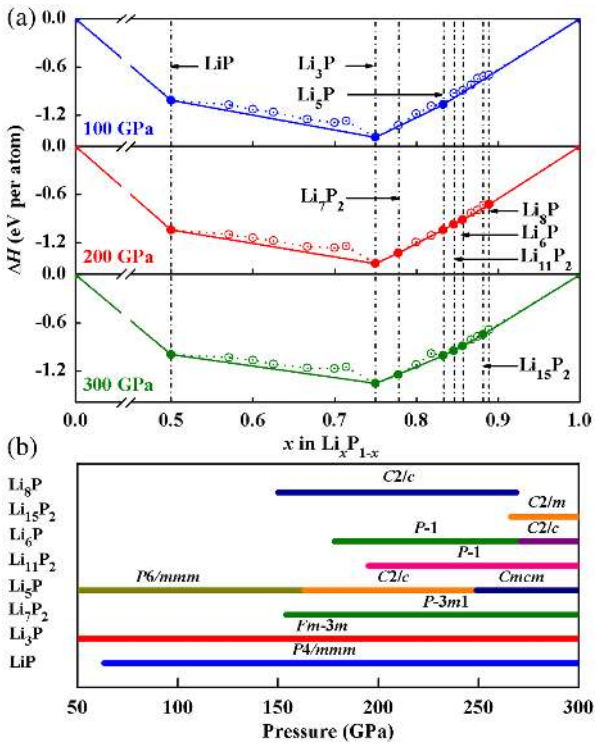

FIG. 1. Relative thermodynamic stability of Li_xP_y at 0 K and different pressures (100, 200, and 300 GPa). (a) The calculated formation enthalpy per atom of Li_xP_y compounds with respect to elemental Li and P solids. The thermodynamically stable compounds are shown by solid symbols, connected by the solid line (convex hull). (b) Pressure-composition phase diagram of Li_xP_y compounds.

phases in Fig. 1(b) are dynamically stable, as they do not show any imaginary frequency modes (Fig. S2 [59]).

Pressure-induced LiP compound stabilizes into a tetragonal structure [space group $P4/mmm$, Fig. 2(a)], in which each P atom has eightfold coordination, with Li atoms forming a P-Li cuboid. As Li content increases, the coordination environment of the P atom changes and it becomes hypercoordinated. P atoms in $P\text{-}3m1$ Li_7P_2 are 14-fold coordinated (Fig. S3a [59]). 15-fold and 17-fold coordinations of P atoms are observed in $C2/c$ Li_5P and $Cmcm$ Li_5P [Figs. 2(b) and 2(c)], respectively; in $P\text{-}1$ $Li_{11}P_2$ (Fig. S3b [59]), $P\text{-}1$ Li_6P [Fig. 2(d)] and $C2/c$ Li_8P [Fig. 2(f)] P atoms show a 16-fold coordination. Notably, the highest coordination appears in $C2/c$ Li_6P [Fig. 2(e)] and $C2/m$ $Li_{15}P_2$ (Fig. S3c [59]), in which P atoms coordinate with 18 nearest-neighbor Li atoms. These coordination numbers are much higher than the previously calculated highest 14-fold coordination in $P6/mmm$ Li_5P [49]. All Li-P phases are compactly assembled P-Li polyhedrons (more detailed structural information can be found in the Supplemental Material [59], Table S1).

Although the P atom is hypercoordinated in all these Li-rich phosphide phases, Bader charge analysis does not conclude it has a hypervalence in any of them (Table S2 [59]). After getting three electrons from Li atoms, P atoms in Li-rich Li_xP_y $(x/y \geq 3)$ fill completely their electronic shells. As a result, the rest of electrons offered by Li atoms accommodate into the lattice spaces, which induces the formation of electrides (Figs. S4 and S5 [59]). The electronic band structures show that these electrides are metallic at the PBE level ($P6/mmm$ Li_5P at 100, $C2/c$ Li_5P at 200, $Cmcm$ Li_5P at 300, $P\text{-}1$ $Li_{11}P_2$ at 200, $P\text{-}1$ Li_6P at 200, $C2/c$ Li_6P at 300, $C2/m$ $Li_{15}P_2$ at 300, and $C2/c$ Li_8P at 200 GPa) [Figs. S6 in the Supplemental Material [59] and Fig. 3(c)]. Additionally, $P4/mmm$ LiP and $P\text{-}3m1$ Li_7P_2, without interstitial electrons, are also metallic, with a dominant contribution of P $3p$ orbital and Li $2p$ orbital (Fig. S7 in Ref. [59]). In contrast, $Fm\text{-}3m$ Li_3P remains insulating until 300 GPa, as a result of a strong ionic bonding between Li and P, due to the high matching among $3Li^+$ and P^{3-} ions, which goes against closing the band.

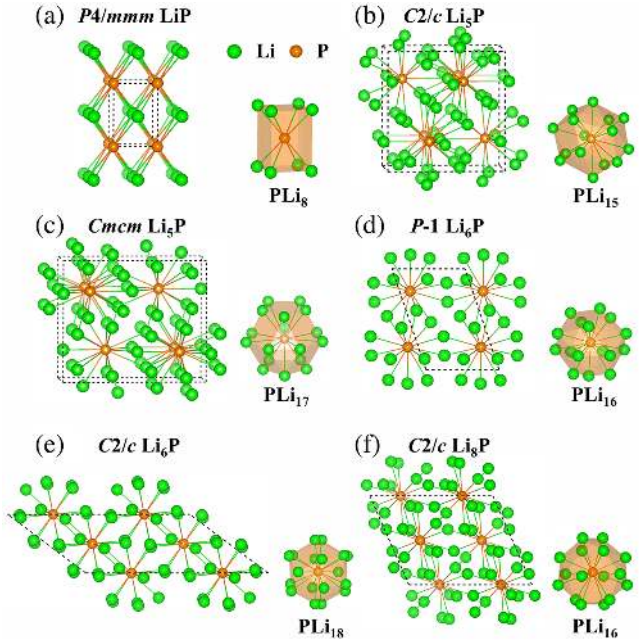

FIG. 2. Structural features of stable Li-P phases at high pressures. (a) $P4/mmm$ LiP at 200 GPa. (b) $C2/c$ Li_5P at 200 GPa. (c) $Cmcm$ Li_5P at 300 GPa. (d) $P\text{-}1$ Li_6P at 200 GPa. (e) $C2/c$ Li_6P at 300 GPa. (f) $C2/c$ Li_8P at 200 GPa. In all these structures, green and orange spheres represent Li and P atoms, respectively.

As difference charge density in Fig. 3(a) clearly shows, excess electrons in the highest coordinated $C2/c$ Li_6P assemble into interstitials on the planes of P atoms, (0 1/3 0), having the dumbbell-like electride states (Fig. S5). More interestingly, these dumbbell-like electride states interconnect each other across intermediate extranuclear electrons of P atoms, which is in sharp contrast with pressure-induced isolated electride states in alkaline and alkaline-earth metals with insulating character [8]. This feature is further supported by its electron localization function (ELF) [63] (Fig. S5 [59]). These connected electronic channels in $C2/c$ Li_6P favor the electronic conductivity, and the contribution of interstitial electrons to the metallic state is illustrated in the projected density of states [PDOS, Fig. 3(d)]. Although the main contribution at the Fermi level comes from Li $2p$ orbital, it has an important contribution associated to the interstitial electrons. In contrast, as P atoms fill their electronic shells by attaining three electrons from Li atoms, P $3s$ and $3p$ orbitals barely reach the Fermi level. As shown in Fig. S8 of Ref. [59], a well-defined Fermi surface nesting appears in Li_6P along $\Gamma \rightarrow M$ [Fig. 3(b)], with highly dispersive bands in this direction [Fig. 3(c)]. Conversely, flatter bands associated to more localized electronic states appear along $\Gamma \rightarrow V$ and $L \rightarrow A$. As discussed above, nearly three electrons in $C2/c$ Li_6P reside in the interstitials. In order to show this, we have built a hypothetical system by removing three electrons from $C2/c$ Li_6P, $[Li_6P]^{3+}$. The absence of interstitial electrons in both ELF and charge density difference of $[Li_6P]^{3+}$ (Figs. S9a and S9b [59]) confirm that these excess electrons are responsible for the electride states.

Motivated by the presence of metallicity in Li-rich Li_xP_y electrides, subsequently, we explore their superconducting transition temperature (T_c) through the McMillan-Allen-Dynes formula [64–66]. Particularly, $C2/c$ Li_6P electride exhibiting Fermi surface nesting and steeply electronic band structure holds a good expectance to be a high-temperature superconductor. Their main superconducting characteristics are shown in Table I. Although metallicity extensively exists in high-pressure Li-P compounds, most of them present a low T_c, except $C2/c$ Li_6P, with a T_c of

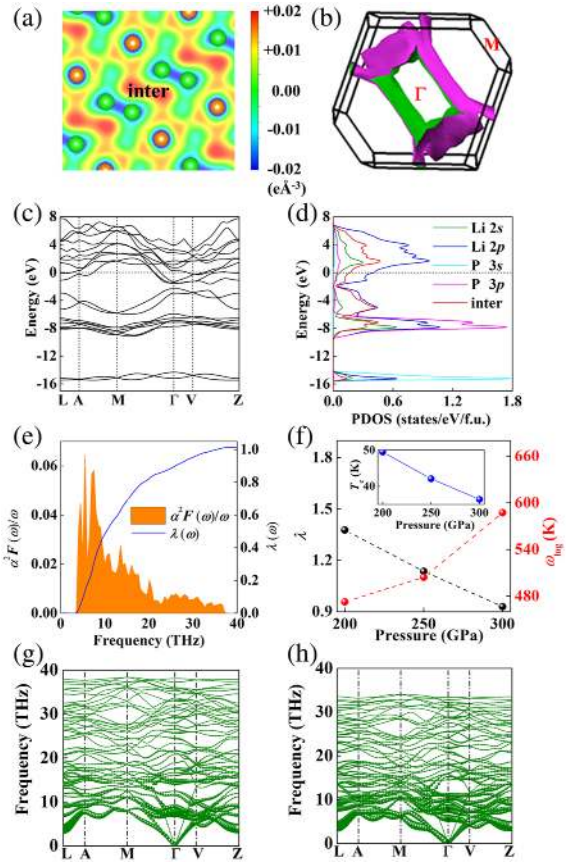

FIG. 3. Electronic and superconducting properties of $C2/c$ Li_6P. (a) Difference charge density (crystal density minus superposition of isolated atomic densities) for $C2/c$ Li_6P plotted on the (0 1/3 0) plane at 300 GPa. (b) The nested Fermi surface along the $\Gamma \rightarrow M$ direction for $C2/c$ Li_6P. The Fermi surface of each band crossing the Fermi energy is shown in Fig. S8 of Ref. [59]. (c) The electronic band structure of $C2/c$ Li_6P at 300 GPa. (d) PDOS of $C2/c$ Li_6P at 300 GPa. The red line labeled by "inter" is obtained by projecting onto the interstitial orbitals (interstitial-site-centered spherical harmonics in empty spheres with a Wigner-Seitz radius of 1.0 Å). (e) Eliashberg spectral function (orange area) and frequency-dependent electron-phonon coupling parameters $\lambda(\omega)$ (blue line) of $C2/c$ Li_6P at 270 GPa. (f) The electron-phonon coupling coefficient λ (black dashed line) and the logarithmic average phonon frequency $\omega_{\log}$ (red dashed line) as a function of pressure. The critical temperature T_c (blue line) as a function of pressure is shown in the inset. The calculated phonon dispersion curves of $C2/c$ Li_6P at 300 (g), and 200 GPa (h). The area of each circle is proportional to the partial electron-phonon coupling, $\lambda_{q,v}$.

39.3 K at 270 GPa. Actually, it is the highest T_c in an electride. The resulting electron-phonon coupling constant λ of $C2/c$ Li_6P is 1.01 at 270 GPa, which is comparable to the maximum value for Li_3S (1.43) [67] and H_2P (1.13) [27]. As can be seen in Fig. 3(e), low-frequency phonon modes dominate superconductivity, so that modes below 10 THz give a contribution of 52.4% to the electron-phonon coupling parameter λ at 270 GPa.

TABLE I. Superconducting properties of the metallic Li-P phases.

Phases	Pressure (GPa)	λ	$\omega_{\log}$ (K)	$N(E_f)$ (states/Ry)	T_c (K)
$C2/c$ Li_5P	200	0.40	634.89	7.41	2.61
$Cmcm$ Li_5P	300	0.25	683.50	4.43	0.05
P-1 $Li_{11}P_2$	200	0.44	670.34	9.73	4.63
P-1 Li_6P	200	0.41	619.35	8.07	2.87
$C2/c$ Li_6P	270	1.01	554.34	11.49	39.30
$C2/m$ $Li_{15}P_2$	300	0.65	637.53	10.55	18.50
$C2/c$ Li_8P	200	0.50	575.54	10.14	7.15

Although $C2/c$ Li_6P is metastable at pressures lower than 270 GPa, in order to better understand the origin of its superconducting T_c, we have analyzed its evolution with pressure. As it is shown in Fig. 3(f), T_c increases as pressure reduces (36.4 K at 300; 49.49 K at 200 GPa), with a pressure coefficient (dT_c/dP) of -0.13 K/GPa. In addition, while λ decreases with pressure, $\omega_{\log}$ increases. As it can be seen in Figs. 3(g) and 3(h), the contribution of low-frequency vibrations to the electron-phonon coupling is reduced with increasing of pressure. Interestingly, the softening along the $\Gamma \rightarrow M$ direction decreases with pressure, which is correlated with the decreasing Fermi surface nesting. This nesting is associated with localized interstitial electrons, which are enhanced under lower pressure (Fig. S10 [59]) and couple more strongly with phonons.

In summary, we have analyzed pressure-induced Li-rich phosphides under pressure up to 300 GPa. Although most of the electrides are nonmetallic, in this work we report that pressure-induced stable Li_5P, $Li_{11}P_2$, Li_6P, $Li_{15}P_2$, and Li_8P compounds are superconducting electrides. Among them, $C2/c$ Li_6P presents a T_c of 39.3 K at 270 GPa, which is the highest among the already known electrides. Superconductivity in these compounds can be attributed to a combination of a weak electronegativity of P with a strong electropositivity of Li. Excess electrons in the highest coordinated $C2/c$ Li_6P assemble into the interstitials on the planes of P atoms forming dumbbell-like anionic electrons, which play a dominant role in the superconducting transition. A Fermi surface nesting associated to localized electronic bands induces a phonon softening that enhances the electron-phonon coupling and favors the superconducting transition. These results open up the interest to explore high-temperature superconductivity in similar binary compounds.

This work is supported by the Natural Science Foundation of China under Grants No. 21573037, No. 21873017, No. 11704062, and No. 51732003; the Natural Science Foundation of Jilin Province (No. 20190201231JC); the Postdoctoral Science Foundation of China (under Grant No. 2013M541283); and the Fundamental Research Funds for the Central

Universities (2412017QD006). A. B. acknowledges financial support from the Spanish Ministry of Economy and Competitiveness (FIS2016-76617-P) and the Department of Education, Universities and Research of the Basque Government and the University of the Basque Country (IT756-13).

*These authors contributed equally to this work.
†Corresponding author.
a.bergara@ehu.eus
‡Corresponding author.
yanggc468@nenu.edu.cn

[1] J. L. Dye, Science **301**, 607 (2003).
[2] C. Park, S. W. Kim, and M. Yoon, Phys. Rev. Lett. **120**, 026401 (2018).
[3] M. S. Miao and R. Hoffmann, J. Am. Chem. Soc. **137**, 3631 (2015).
[4] M. S. Miao and R. Hoffmann, Acc. Chem. Res. **47**, 1311 (2014).
[5] M. S. Miao, X. L. Wang, J. Brgoch, F. Spera, M. G. Jackson, G. Kresse, and H. Q. Lin, J. Am. Chem. Soc. **137**, 14122 (2015).
[6] C. J. Pickard and R. J. Needs, Phys. Rev. Lett. **102**, 146401 (2009).
[7] M. Martinez-Canales, C. J. Pickard, and R. J. Needs, Phys. Rev. Lett. **108**, 045704 (2012).
[8] Y. Ma, M. Eremets, A. R. Oganov, Y. Xie, I. Trojan, S. Medvedev, A. O. Lyakhov, M. Valle, and V. Prakapenka, Nature (London) **458**, 182 (2009).
[9] P. Li, G. Gao, Y. Wang, and Y. Ma, J. Phys. Chem. C **114**, 21745 (2010).
[10] Y. Lu, J. Li, T. Tada, Y. Toda, S. Ueda, T. Yokoyama, M. Kitano, and H. Hosono, J. Am. Chem. Soc. **138**, 3970 (2016).
[11] J. Park, K. Lee, S. Y. Lee, C. N. Nandadasa, S. Kim, K. H. Lee, Y. H. Lee, H. Hosono, S. G. Kim, and S. W. Kim, J. Am. Chem. Soc. **139**, 615 (2017).
[12] J. Wang, K. Hanzawa, H. Hiramatsu, J. Kim, N. Umezawa, K. Iwanaka, T. Tada, and H. Hosono, J. Am. Chem. Soc. **139**, 15668 (2017).
[13] Y. Tsuji, P. L. V. K. Dasari, S. F. Elatresh, R. Hoffmann, and N. W. Ashcroft, J. Am. Chem. Soc. **138**, 14108 (2016).
[14] Y. Zhang, W. Wu, Y. Wang, S. A. Yang, and Y. Ma, J. Am. Chem. Soc. **139**, 13798 (2017).
[15] Y. Zhang, B. Wang, Z. Xiao, Y. Lu, T. Kamiya, Y. Uwatoko, H. Kageyama, and H. Hosono, npj Quantum Mater. **2**, 45 (2017).
[16] E. W. Huang, C. B. Mendl, S. Liu, S. Johnston, H. C. Jiang, B. Moritz, and T. P. Devereaux, Science **358**, 1161 (2017).
[17] E. H. da Silva Neto, M. Minola, B. Yu, W. Tabis, M. Bluschke, D. Unruh, H. Suzuki, Y. Li, G. Yu, D. Betto, K. Kummer, F. Yakhou, N. B. Brookes, M. Le Tacon, M. Greven, B. Keimer, and A. Damascelli, Phys. Rev. B **98**, 161114(R) (2018).
[18] Q. Si, R. Yu, and E. Abrahams, Nat. Rev. Mater. **1**, 16017 (2016).
[19] H. Hosono, A. Yamamoto, H. Hiramatsu, and Y. Ma, Mater. Today **21**, 278 (2018).
[20] G. Profeta, C. Franchini, N. N. Lathiotakis, A. Floris, A. Sanna, M. A. L. Marques, M. Luders, S. Massidda, E. K. U. Gross, and A. Continenza, Phys. Rev. Lett. **96**, 047003 (2006).
[21] N. W. Ashcroft, Phys. Rev. Lett. **92**, 187002 (2004).
[22] Y. Li, J. Hao, H. Liu, Y. Li, and Y. Ma, J. Chem. Phys. **140**, 174712 (2014).
[23] D. Duan, X. Huang, F. Tian, D. Li, H. Yu, Y. Liu, Y. Ma, B. Liu, and T. Cui, Phys. Rev. B **91**, 180502(R) (2015).
[24] A. P. Drozdov, M. I. Eremets, I. A. Troyan, V. Ksenofontov, and S. I. Shylin, Nature (London) **525**, 73 (2015).
[25] J. A. Flores-Livas, M. Amsler, C. Heil, A. Sanna, L. Boeri, G. Profeta, C. Wolverton, S. Goedecker, and E. K. U. Gross, Phys. Rev. B **93**, 020508(R) (2016).
[26] Y. Fu, X. Du, L. Zhang, F. Peng, M. Zhang, C. J. Pickard, R. J. Needs, D. J. Singh, W. Zheng, and Y. Ma, Chem. Mater. **28**, 1746 (2016).
[27] A. Shamp, T. Terpstra, T. Bi, Z. Falls, P. Avery, and E. Zurek, J. Am. Chem. Soc. **138**, 1884 (2016).
[28] H. Liu, Y. Li, G. Gao, J. S. Tse, and I. I. Naumov, J. Phys. Chem. C **120**, 3458 (2016).
[29] A. P. Drozdov, M. I. Eremets, and I. A. Troyan, arXiv: 1508.06224.
[30] H. Liu, I. I. Naumov, R. Hoffmann, N. W. Ashcroft, and R. J. Hemley, Proc. Natl. Acad. Sci. U.S.A. **114**, 6990 (2017).
[31] F. Peng, Y. Sun, C. J. Pickard, R. J. Needs, Q. Wu, and Y. Ma, Phys. Rev. Lett. **119**, 107001 (2017).
[32] M. Somayazulu, M. Ahart, A. K. Mishra, Z. M. Geballe, M. Baldini, Y. Meng, V. V. Struzhkin, and R. J. Hemley, Phys. Rev. Lett. **122**, 027001 (2019).
[33] M. Miyakawa, S. W. Kim, M. Hirano, Y. Kohama, H. Kawaji, T. Atake, H. Ikegami, K. Kono, and H. Hosono, J. Am. Chem. Soc. **129**, 7270 (2007).
[34] T. N. Ye, J. Li, M. Kitano, and H. Hosono, Green Chem. **19**, 749 (2017).
[35] Y. Kohama, S. W. Kim, T. Tojo, H. Kawaji, T. Atake, S. Matsuishi, and H. Hosono, Phys. Rev. B **77**, 092505 (2008).
[36] Y. Toda, Y. Kubota, M. Hirano, H. Hirayama, and H. Hosono, ACS Nano **5**, 1907 (2011).
[37] Y. Ge, S. Guan, and Y. Liu, New J. Phys. **19**, 123020 (2017).
[38] Y. Yao, J. S. Tse, and D. D. Klug, Phys. Rev. Lett. **102**, 115503 (2009).
[39] C. L. Guillaume, E. Gregoryanz, O. Degtyareva, M. I. McMahon, M. Hanfland, S. Evans, M. Guthrie, S. V. Sinogeikin, and H. K. Mao, Nat. Phys. **7**, 211 (2011).
[40] A. R. Oganov, Y. Ma, Y. Xu, I. Errea, A. Bergara, and A. O. Lyakhov, Proc. Natl. Acad. Sci. U.S.A. **107**, 7646 (2010).
[41] M. Gatti, I. V. Tokatly, and A. Rubio, Phys. Rev. Lett. **104**, 216404 (2010).
[42] M. Marqués, M. I. McMahon, E. Gregoryanz, M. Hanfland, C. L. Guillaume, C. J. Pickard, G. J. Ackland, and R. J. Nelmes, Phys. Rev. Lett. **106**, 095502 (2011).
[43] X. Dong, Y.-L. Li, A. R. Oganov, K. Li, H. Zheng, and H.-k. Mao, arXiv:1603.02880.
[44] R. Zhang, J. Waters, A. K. Geim, and I. V. Grigorieva, Nat. Commun. **8**, 15036 (2017).
[45] J. A. Flores Livas, A. Sanna, A. P. Drozdov, L. Boeri, G. Profeta, M. Eremets, and S. Goedecker, Phys. Rev. Mater. **1**, 024802 (2017).

[46] C. M. Park and H. J. Sohn, Adv. Mater. **19**, 2465 (2007).
[47] X. Ren, P. Lian, D. Xie, Y. Yang, Y. Mei, X. Huang, Z. Wang, and X. Yin, J. Mater. Sci. **52**, 10364 (2017).
[48] M. Mayo, K. J. Griffith, C. J. Pickard, and A. J. Morris, Chem. Mater. **28**, 2011 (2016).
[49] Z. Zhao, L. Liu, T. Yu, G. Yang, and A. Bergara, J. Phys. Chem. C **121**, 21199 (2017).
[50] Y. Wang, J. Lv, L. Zhu, and Y. Ma, Phys. Rev. B **82**, 094116 (2010).
[51] Y. Wang, J. Lv, L. Zhu, and Y. Ma, Comput. Phys. Commun. **183**, 2063 (2012).
[52] W. Kohn and L. J. Sham, Phys. Rev. **140**, A1133 (1965).
[53] P. Hohenberg and W. Kohn, Phys. Rev. **136**, B864 (1964).
[54] J. P. Perdew, K. Burke, and M. Ernzerhof, Phys. Rev. Lett. **77**, 3865 (1996).
[55] G. Kresse and J. Furthmüller, Phys. Rev. B **54**, 11169 (1996).
[56] P. E. Blöchl, Phys. Rev. B **50**, 17953 (1994).
[57] J. D. Pack and H. J. Monkhorst, Phys. Rev. B **16**, 1748 (1977).
[58] P. Giannozzi, S. Baroni, N. Bonini, M. Calandra, R. Car, C. Cavazzoni, D. Ceresoli, G. L. Chiarotti, M. Cococcioni, and I. Dabo, J. Phys. Condens. Matter **21**, 395502 (2009).
[59] See Supplemental Material at http://link.aps.org/supplemental/10.1103/PhysRevLett.122.097002 for computational details, the convex hull of Li-P system at 50 GPa, structural features of Li_7P_2, $Li_{11}P_2$, and $Li_{15}P_2$, phonon dispersion curves, electronic properties, structural information, and Bader charge analysis of Li-P phases, which includes Refs. [60–62].
[60] P. Blaha, K. Schwarz, P. Sorantin, and S. B. Trickey, Comput. Phys. Commun. **59**, 399 (1990).
[61] P. B. Allen and B. Mitrović, Solid State Phys. **37**, 1 (1983).
[62] J. P. Carbotte, Rev. Mod. Phys. **62**, 1027 (1990).
[63] A. D. Becke and K. E. Edgecombe, J. Chem. Phys. **92**, 5397 (1990).
[64] L. N. Oliveira, E. K. U. Gross, and W. Kohn, Phys. Rev. Lett. **60**, 2430 (1988).
[65] M. Lüders, M. A. L. Marques, N. N. Lathiotakis, A. Floris, G. Profeta, L. Fast, A. Continenza, S. Massidda, and E. K. U. Gross, Phys. Rev. B **72**, 024545 (2005).
[66] M. A. L. Marques, M. Lüders, N. N. Lathiotakis, G. Profeta, A. Floris, L. Fast, A. Continenza, E. K. U. Gross, and S. Massidda, Phys. Rev. B **72**, 024546 (2005).
[67] C. Kokail, C. Heil, and L. Boeri, Phys. Rev. B **94**, 060502(R) (2016).